Lagrangian Descriptors of Thermalized Transition States on Time-Varying Energy Surfaces

Galen T. Craven and Rigoberto Hernandez*
Center for Computational Molecular Science and Technology, School of Chemistry and Biochemistry, Georgia Institute of Technology, Atlanta, Georgia 30332-0400, USA
(Received 1 May 2015; published 29 September 2015)

Thermalized chemical reactions driven under dynamical load are characteristic of activated dynamics for arbitrary nonautonomous systems. Recent generalizations of transition state theory to obtain formally exact rates have required the construction of a time-dependent transition state trajectory. Here, we show that Lagrangian descriptors can be used to obtain this structure directly. By developing a phase space separatrix that is void of recrossings, these constructs allow for the principal criterion in the implementation of modern rate theories to be satisfied. Thus, the reactive flux over a time-varying barrier can be determined without ambiguity in chemical reactions. The generality of the formalism suggests that this approach is applicable to any activated system subjected to arbitrary driving and thermal fluctuations.

DOI: 10.1103/PhysRevLett.115.148301 PACS numbers: 82.20.Db, 05.40.Ca, 05.45.-a, 34.10.+x

Paramount in the formulation of the theory for chemical reaction dynamics is the control of rates, and routes through which reactants transform to products. The emergence of phenomena driven under a dynamical load—such as molecular structure assembly [1,2], molecular machines [3,4], mechanochemistry [5–7], and electric field-induced reactions [8–10]—has demonstrated that novel products can be realized through nonequilibrium forcing. Such phenomena can be captured through nonequilibrium thermodynamic models in which external forces are represented by time-varying energy surfaces [11–14]. They have been observed experimentally in the control of state-to-state transitions through mechanical or temperature modulated energy surfaces in biologically relevant systems [15–17]. In these directed processes, the rates of the reaction can be obtained from purely geometrical arguments through transition state theory (TST) [18–23]. The principal step in the application of TST, and its variants, relies on the calculation of reactive flux through a dividing surface (DS) that separates reactant and product confirmations. In cases where this DS is a surface of no return, TST is formally exact.

In autonomous Hamiltonian systems, the formulation of normally hyperbolic invariant manifolds (NHIMs) [24–30] has provided a critical step toward the construction of optimal dividing surfaces. The study of NHIMs is a focus of modern reaction dynamics as knowledge of their geometry allows *a priori* determination of the characteristics of the reaction. However, a distinguishing feature of microscale molecular systems, with respect to macroscopic dynamical counterparts, is the inclusion of thermal fluctuations, and in a fluctuating environment, the formulation of the NHIM as a constant energy hypersphere breaks down. Thus, in solution and on time-varying energy surfaces, the construction of reaction geometries has generally been limited to theoretical constructs and localized approximations. In this Letter, we report a methodology for obtaining a surface of no return and the attached reaction conduits on time-varying potential energy surfaces subject to thermal fluctuations, described through a Langevin equation, using the method of Lagrangian descriptors (LDs). This opens up the possibility of addressing dissipative activation processes and chemical reactions on complex energy landscapes far from the near-linear regimes that have been accessible through perturbation theory. It also enables the determination of exact rates for processes occurring on time-varying energy landscapes using the calculation of the reactive flux through the DS.

The general form of a LD [31,32] is

$$M(\mathbf{q}_0, t_0)_\tau = \int_{t_0-\tau}^{t_0+\tau} \mathcal{P}(\mathbf{q}(t))dt, \tag{1}$$

where $\mathcal{P}$ is a bounded positive quantity that depends on the unique trajectory $\mathbf{q}(t)$ which evolved from $\mathbf{q}_0$ at time t_0. The application of LDs to nonautonomous systems has provided insight into the phase space structures governing dynamical evolution in aperiodically modulated fields [32], including ocean flow patterns [31]. At microscopic length scales, thermal forces arise from solvent-reactant and reactant-reactant interactions. In a large number of known cases [33], the dynamics can be represented through a Langevin equation of motion with respect to some characteristic configuration variable q as

$$m\ddot{q} = -\gamma\dot{q} - \frac{\partial V(q,t)}{\partial q} + \sqrt{2\sigma}\xi_\alpha(t), \tag{2}$$

where $\gamma \geq 0$ is a dissipation parameter and the stochastic term $\xi_\alpha(t)$ is white noise obeying the statistical properties $\langle \xi_\alpha(t) \rangle = 0$ and $\langle \xi_\alpha(t)\xi_\alpha(t') \rangle = \delta(t-t')$ for some noise

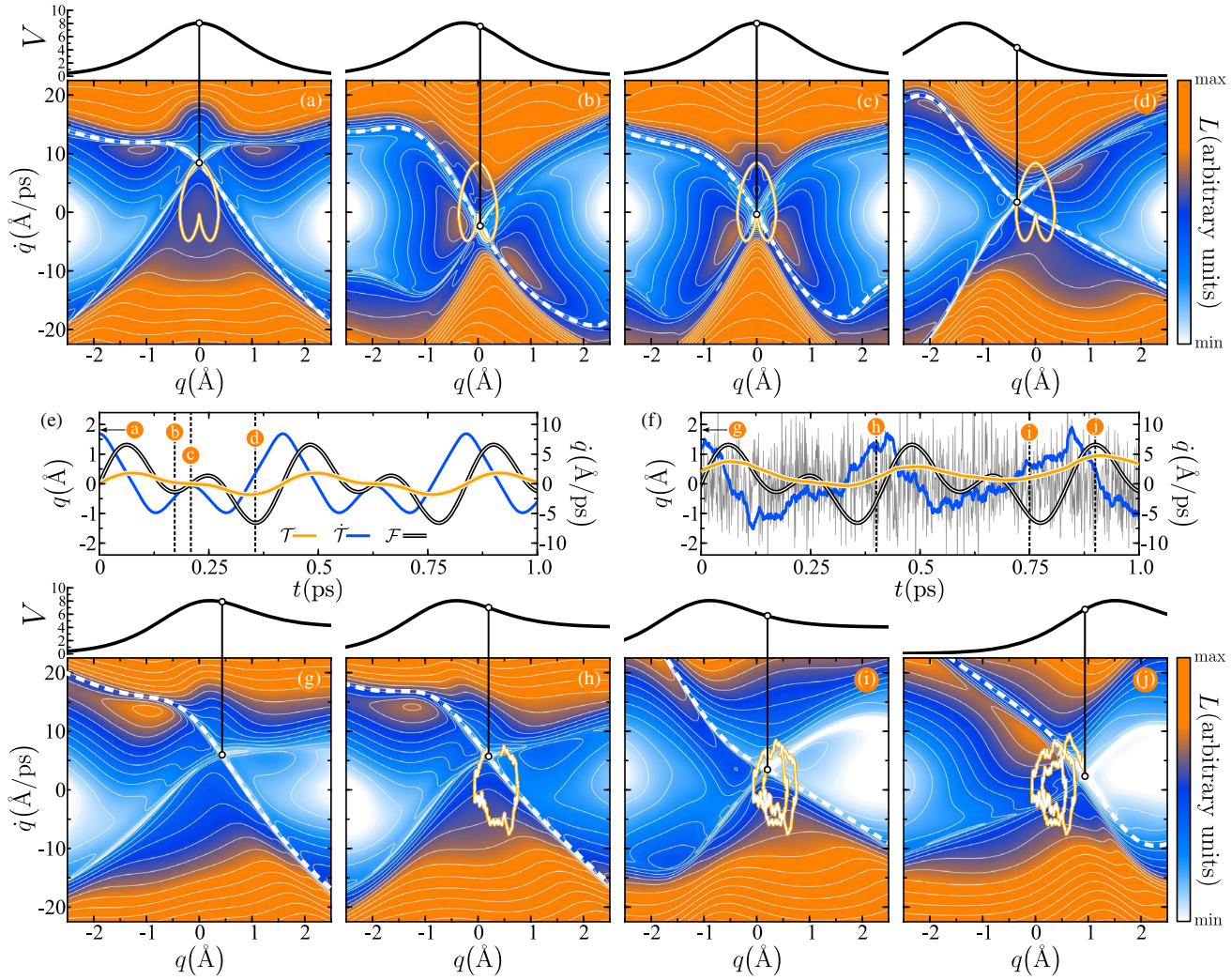

FIG. 1 (color online). Phase space contour plots of $L(\mathbf{q}_0, t_0)$ for varying values of t_0 are shown in (a)–(d) for a symmetrical barrier ($\kappa = 1, \gamma = 0$) and in (g)–(j) for a thermalized asymmetrical barrier ($\kappa = 0.5, \gamma = 25\ m_u/\text{ps}$). In all panels, the TS trajectory $\boldsymbol{\mathcal{T}}(t)$ is shown as a striped curve (white-orange) and the stable manifold is shown as a dashed curve (white). In the athermal case, $\boldsymbol{\mathcal{T}}$ is shown over an entire period of oscillation, while in the thermal case, it is shown over the interval $[0, t_0]$. The time-varying potential surface is shown above in units of $k_B T$ at 298 K, which is the temperature of the thermal bath. The corresponding values of t_0 are marked in (e) and (f) for thermal and athermal cases, respectively, with trajectories of $\mathcal{T}$, $\mathcal{F}$, as well as $\dot{\mathcal{T}}$ (units shown at right). The thermal driving (gray) given by $\int_t^{t+\Delta t} \xi_\alpha(t')dt'$ is shown in (f) for each integration time step $\Delta t = 0.001$ ps [36]. Parameters in all panels are $\tau = 0.5$ ps, $m = 10\, m_u$, $c_1 = c_2 = 0.75$ Å, $\Omega_1 = 15$ ps^{-1}, $a = 0.85$ Å^{-1}, and $\tau_w = 0.2$ ps.

sequence α. The thermal degrees of freedom are expressed in terms of the stochastic mean field ξ_α whose strength is varied through the parameter $\sigma = \gamma k_B T$, thus obeying a fluctuation-dissipation relation.

When a reaction is subjected to a time-varying external force, a nonautonomous TS persists [34,35] and corresponds to a moving bottleneck in phase space through which reactive trajectories must pass as a product is formed. The Eckart barrier is often used to represent molecular reactions under stationary conditions for a given asymmetry parameter κ representing the energy difference between reactants and products. It can be generalized to a time-varying form (see Fig. 1),

$$V(q,t) = \frac{V_0(1-\kappa)}{1+\exp[-2a(q-\mathcal{F}(t))]} + \frac{V_0(1+\sqrt{\kappa})^2}{4}\,\mathrm{sech}^2[a(q-\mathcal{F}(t))], \quad (3)$$

so as to separate reactants and products along a generalized coordinate q subject to an external time-varying forcing $\mathcal{F}(t)$. Here, we consider the case when variations in the energy surface $V(q,t)$ result from a bichromatic driving form $\mathcal{F}(t) = c_1 \sin(\Omega_1 t) + c_2 \sin(\Omega_2 t)$ which is periodic, with a resonant frequency $\Omega_2 = 2\Omega_1$.

Every noise sequence $\xi_\alpha(t)$, coupled with the realization of the deterministic forcing $\mathcal{F}(t)$, has a hyperbolic

trajectory $\mathcal{T}(t)$ [37–39] hidden in the phase space structure that mediates reactive flow. In the field of chemical reaction dynamics, this trajectory has been termed the TS trajectory [40–42], and a DS attached to this trajectory is free of recrossings. Despite its paramount importance, constructing the TS trajectory in thermal environments has been previously limited to parabolic barrier approximations, thus limiting the applicability of TST on energy surfaces subjected to thermal fluctuations.

As illustrated in Fig. 1, on time-varying energy surfaces, frozen-time vector fields [38,43] provide little insight into the complex geometry of the TS trajectory, which does not follow the time evolution of the energetic barrier top (BT). Instead, the TS trajectory is bounded and associated with stable $\mathcal{W}^s$ and unstable manifolds $\mathcal{W}^u$ which separate reactive and nonreactive basins in phase space. These manifolds are formed by the set of initial conditions, at a time t_0, of trajectories that approach $\mathcal{T}(t)$ as $t \to \infty$ and $t \to -\infty$, respectively. When $\mathcal{F}(t)$ is a periodic function, and the barrier motion is athermal ($\gamma = 0$), the resulting TS trajectory is a periodic orbit $\mathcal{O}$ which has the same period as $\mathcal{F}(t)$ [see Figs. 1(a)–1(e)]. In a thermal environment ($\gamma > 0$ and $T > 0$), $\mathcal{T}(t)$ will depend on the strength of the thermal fluctuations (parametrized through σ) and the specific noise sequence, as shown in Figs. 1(f)–1(j).

To construct the TS trajectory and associated manifolds, we note that it is the only trajectory that remains bounded as $t \to \infty$ and as $t \to -\infty$. Thus, it has extremal properties; e.g., it is the trajectory with the minimum arc length over sufficient propagation. The LDs that correspond to the arc length of the path traversed in configuration space over a time τ are

$$L_{f,b}(\mathbf{q}_0, t_0)_\tau = \int_{f,b} \|\dot{\mathbf{q}}_c(\mathbf{q}_0, t_0, t)\| dt, \tag{4}$$

where the intervals of forward "f" and backward "b" integration are $[t_0, t_0 + \tau]$ and $[t_0 - \tau, t_0]$, $\|\cdot\|$ is the Euclidean metric, and $\mathbf{q}_c$ are generalized coordinates. In the nonautonomous system given by Eq. (2), the manifolds associated with the TS trajectory $\mathcal{T}$ are also time dependent. For the case of a barrier (3) separating reactant and product states, in a suitable phase space region R_f, holding the coordinate q_0 constant and minimizing with respect to $\dot{q}_0$ yields the stable manifold

$$\mathcal{W}^s(q_0 = C, t_0) = \text{argmin}\, L_f(\dot{q}_0, q_0 = C, t_0)_{R_f}, \tag{5}$$

in forward time, and the unstable manifold

$$\mathcal{W}^u(q_0 = C, t_0) = \text{argmin}\, L_b(\dot{q}_0, q_0 = C, t_0)_{R_b}, \tag{6}$$

in backward time about the region R_b, where argmin$(\cdot)$ is the argument of the minimum function; i.e., we seek the value of $\dot{q}_0$ that minimizes $L_{f,b}$ while holding q_0 constant. The TS trajectory can then be constructed by finding the extrapolated point of intersection between $\mathcal{W}^s$ and $\mathcal{W}^u$ at each time t. Alternatively, a minimization procedure can be performed over an object that combines forward- and backward-time information, namely, $L = L_f + L_b$. The phase space coordinates of the TS trajectory at t_0 can then be constructed directly as

$$\mathcal{T}(t_0) = \text{argmin}\, L(\mathbf{q}_0, t_0)_{R_f \cap R_b}, \tag{7}$$

as it is the unique trajectory that remains bounded for all time [44].

A dissipative environment leads to exponential contraction and growth in the phase space volumes for the evolution of forward and backward trajectories, respectively. To avoid

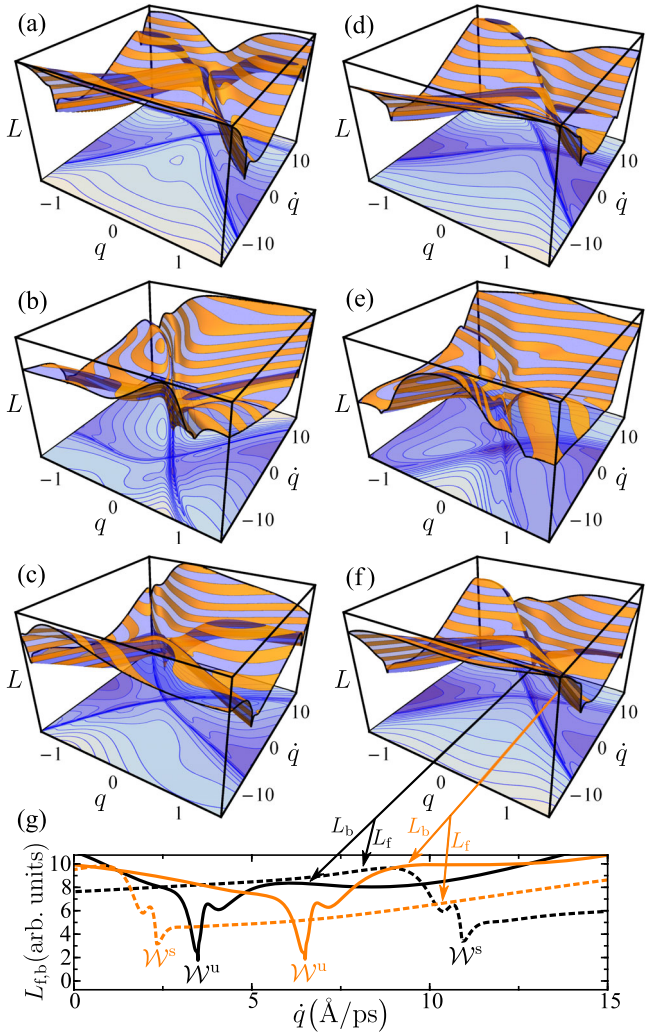

FIG. 2 (color online). Surfaces formed by $L(\mathbf{q}_0, t_0)$ with $\tau = 0.5$ ps are shown above for athermal symmetrical (a)–(c) and thermalized asymmetrical (d)–(f) barriers with the corresponding contour plot shown below in each panel. The initial times are (from top to bottom) $t_0 \in \{0, 0.129, 0.356\}$ (left panel) and $t_0 \in \{0, 0.209, 0.4\}$ (right panel). All units and parameters are as in Fig. 1. (g) Calculation of $L_{f,b}$ with q_0 held constant at the marked values and $\tau = 0.75$ ps.

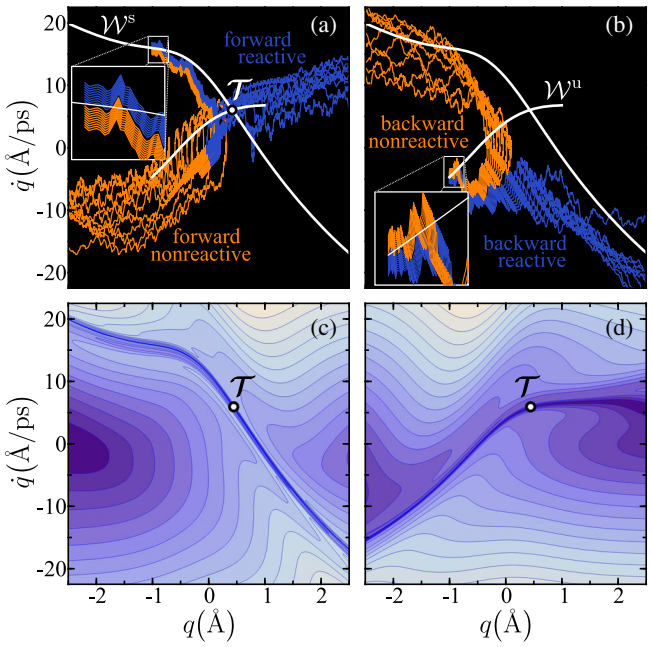

FIG. 3 (color online). Phase portraits of (a) forward-time and (b) backward-time integration of an ensemble of trajectories in a thermal environment. The initial position for every trajectory is $q_0 = -1$ Å. Pieces of the stable $\mathcal{W}^s$ and unstable $\mathcal{W}^u$ manifolds at $t_0 = 0$ are shown in white and marked accordingly. Contour plots of the forward-time and backward-time surface $L_{f,b}$ with $\tau = 1.0$ ps are shown in (c) and (d), respectively. Parameters in all panels are as in the asymmetrical thermalized case in Fig. 1.

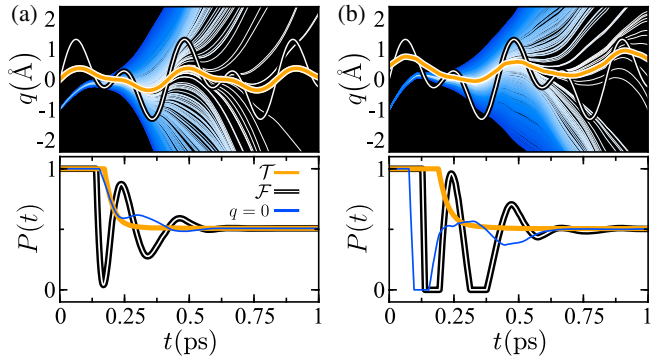

FIG. 4 (color online). Time evolution of a swarm of trajectories in (a) athermal and (b) thermal environments. Each trajectory is colored according to the difference in initial velocity with respect to the stable manifold at $q_0 = \mathcal{T}(0) - 1$ Å and $t_0 = 0$. The trajectories of two dividing surfaces: the TS trajectory (orange) and the instantaneous BT (striped black) are also shown. The respective reactant populations P for each choice of dividing surface and the additional static surface $q = 0$ are shown below. The system parameters are as in Fig. 1.

the dominant contribution of L_b, we renormalize the arc length as $L = g_f L_f + g_b L_b$, where $g_{f,b}$ are weights. To compensate for the exponential behavior of dissipation, we have chosen $g_{f,b} = e^{\pm\gamma\tau_w/m}$ for some characteristic intermediate time τ_w where the typical contributions from L_b and L_f are comparable over an ensemble of trajectories. After this weighing procedure, the instantaneous structures of the manifolds are revealed as valleys on the L surface, as shown in Fig. 2 [45]. Most importantly, about the region of intersection between the stable and unstable manifolds $R_f \cap R_b$, a conical structure emerges with the vertex corresponding to $\boldsymbol{\mathcal{T}}$. As shown in Figs. 3(a) and 3(b), the stable (unstable) manifold separates reactive and nonreactive trajectories in forward (backward) time. Thus, the construction of these reaction conduits through a minimization procedure on $L_{f,b}$ reveals the phase space geometries [see Figs. 3(c) and 3(d)] separating phase space basins.

The principal steps in the implementation of modern reaction rate theory are the construction of a DS that is crossed once and only once by reactive trajectories, and the evaluation of the reactive flux through the DS. If a surface of no return can be constructed, a classically exact reaction rate can be obtained [20]. For the thermalized reactive system evolving through Eq. (2), we construct a time-dependent DS that is located at the instantaneous position of the TS trajectory. This DS is free of recrossings in periodically driven [34,35], athermal systems [see Fig. 4(a)]. We now examine the validity of the DS constructed by minimizing Eq. (4) in any thermal environment by focusing on the reaction dynamics of an ensemble of trajectories. Each trajectory has an initial position q_0 in the reactant well and an initial velocity sampled from a uniform distribution $\mathcal{U}[\mathcal{W}^s(q_0, 0) - 1$ Å/ps, $\mathcal{W}^s(q_0, 0) + 1$ Å/ps]. The survival probability of each trajectory is followed in time to compute the normalized reactant population $P(t) = n_R(t)/N$, where $n_R(t)$ is the number of trajectories in the reactant well at time t and N is the total number of trajectories. The decay rate of $P(t)$ depends on the choice of DS, and a recrossing-free DS results in monotonically decreasing behavior. The use of the instantaneous energetic BT as the DS results in oscillatory behavior due to recrossings. As shown in Fig. 4, when using the BT as the DS, the functional shape of $P(t)$ mimics the oscillatory driving motion. This behavior can also be seen in parabolic systems [40–42] where the TS trajectory has a smaller amplitude than the barrier motion itself [34,46]. The use of the naive static surface $q = 0$ leads to significant recrossings that are strongly dependent on the specific realization of the noise ξ_α. This is in sharp contrast to the monotonic behavior shown in Fig. 4(b) using the DS constructed by the method of extremal LDs, and thereby illustrating the nonrecrossing criterion.

In summary, we have developed a minimal and robust methodology through the use of an extremal Lagrangian descriptor to construct phase space separatrices and surfaces of no return on time-varying energy surfaces subjected to thermal fluctuations. These findings allow for the classically exact calculation of reactive flux through a recrossing-free dividing surface and have suitable applications in the development and implementation of modern and post-modern transition state theories. The results

reported here are obtained in the physical context of reaction dynamics, although they are also applicable to other dynamical systems in which noise plays a role. The methods are generalizable over variation in geometry of the potential and realization of the driving form. Controlling the hyperbolic trajectories [38,39,47] and the associated manifolds constructed in this Letter provides a critical step toward optimal control of reaction rates and mechanisms, and could, in the context of a general theoretical formulation, facilitate the design of novel synthetic products and materials.

This work has been supported by the Air Force Office of Scientific Research through Grant No. FA9550-12-1-0483. We thank Thomas Bartsch, Fabio Revuelta, and Andrej Junginger for insightful discussions.

*To whom all correspondence should be addressed.
hernandez@chemistry.gatech.edu

[1] A. Prokop, J. Vacek, and J. Michl, ACS Nano **6**, 1901 (2012).
[2] F. Ma, D. T. Wu, and N. Wu, J. Am. Chem. Soc. **135**, 7839 (2013).
[3] S.-H. Lee and D. G. Grier, J. Phys. Condens. Matter **17**, S3685 (2005).
[4] J. Neumann, K. E. Gottschalk, and R. D. Astumian, ACS Nano **6**, 5242 (2012).
[5] Y. Suzuki and O. K. Dudko, Phys. Rev. Lett. **104**, 048101 (2010).
[6] M. Hinczewski, J. C. M. Gebhardt, M. Rief, and D. Thirumalai, Proc. Natl. Acad. Sci. U.S.A. **110**, 4500 (2013).
[7] I. Benichou and S. Givli, Phys. Rev. Lett. **114**, 095504 (2015).
[8] S. Kawai and T. Komatsuzaki, J. Chem. Phys. **134**, 024317 (2011).
[9] D. Blazevski and R. de la Llave, J. Phys. A **44**, 195101 (2011).
[10] D. Blazevski and J. Franklin, Chaos **22**, 043138 (2012).
[11] T. Harada and S.-I. Sasa, Phys. Rev. Lett. **95**, 130602 (2005).
[12] F. R. N. Koch, F. Lenz, C. Petri, F. K. Diakonos, and P. Schmelcher, Phys. Rev. E **78**, 056204 (2008).
[13] J. R. Gomez-Solano, A. Petrosyan, S. Ciliberto, R. Chetrite, and K. Gawedzki, Phys. Rev. Lett. **103**, 040601 (2009).
[14] M. Gärttner, F. Lenz, C. Petri, F. K. Diakonos, and P. Schmelcher, Phys. Rev. E **81**, 051136 (2010).
[15] J. Morfill, J. Neumann, K. Blank, U. Steinbach, E. M. Puchner, K.-E. Gottschalk, and H. E. Gaub, J. Mol. Biol. **381**, 1253 (2008).
[16] H. Gelman, M. Platkov, and M. Gruebele, Chem. Eur. J. **18**, 6420 (2012).
[17] M. Platkov and M. Gruebele, J. Chem. Phys. **141**, 035103 (2014).
[18] R. Hernandez, J. Chem. Phys. **101**, 9534 (1994).
[19] T. Komatsuzaki and R. S. Berry, Proc. Natl. Acad. Sci. U.S.A. **98**, 7666 (2001).
[20] H. Waalkens, R. Schubert, and S. Wiggins, Nonlinearity **21**, R1 (2008).
[21] T. Bartsch, J. M. Moix, R. Hernandez, S. Kawai, and T. Uzer, Adv. Chem. Phys. **140**, 191 (2008).
[22] R. Hernandez, T. Bartsch, and T. Uzer, Chem. Phys. **370**, 270 (2010).
[23] S. Kawai and T. Komatsuzaki, Phys. Rev. Lett. **105**, 048304 (2010).
[24] E. Pollak and P. Pechukas, J. Chem. Phys. **69**, 1218 (1978).
[25] P. Pechukas and E. Pollak, J. Chem. Phys. **71**, 2062 (1979).
[26] T. Uzer, C. Jaffé, J. Palacián, P. Yanguas, and S. Wiggins, Nonlinearity **15**, 957 (2002).
[27] H. Teramoto, M. Toda, and T. Komatsuzaki, Phys. Rev. Lett. **106**, 054101 (2011).
[28] C.-B. Li, A. Shoujiguchi, M. Toda, and T. Komatsuzaki, Phys. Rev. Lett. **97**, 028302 (2006).
[29] H. Waalkens and S. Wiggins, J. Phys. A **37**, L435 (2004).
[30] U. Çiftçi and H. Waalkens, Phys. Rev. Lett. **110**, 233201 (2013).
[31] C. Mendoza and A. M. Mancho, Phys. Rev. Lett. **105**, 038501 (2010).
[32] A. M. Mancho, S. Wiggins, J. Curbelo, and C. Mendoza, Commun. Nonlinear Sci. Numer. Simul. **18**, 3530 (2013).
[33] R. Zwanzig, *Nonequilibrium Statistical Mechanics* (Oxford University Press, London, 2001).
[34] G. T. Craven, T. Bartsch, and R. Hernandez, Phys. Rev. E **89**, 040801(R) (2014).
[35] G. T. Craven, T. Bartsch, and R. Hernandez, J. Chem. Phys. **142**, 074108 (2015).
[36] The integration was performed using a Runga-Kutta-Maruyama fourth-order scheme.
[37] A. M. Mancho, D. Small, S. Wiggins, and K. Ide, Physica D (Amsterdam) **182**, 188 (2003).
[38] J. A. Jiménez Madrid and A. M. Mancho, Chaos **19**, 013111 (2009).
[39] S. Balasuriya and K. Padberg-Gehle, Phys. Rev. E **90**, 032903 (2014).
[40] T. Bartsch, R. Hernandez, and T. Uzer, Phys. Rev. Lett. **95**, 058301 (2005).
[41] T. Bartsch, T. Uzer, and R. Hernandez, J. Chem. Phys. **123**, 204102 (2005).
[42] T. Bartsch, T. Uzer, J. M. Moix, and R. Hernandez, J. Chem. Phys. **124**, 244310 (2006).
[43] A. M. Mancho, D. Small, and S. Wiggins, Phys. Rep. **437**, 55 (2006).
[44] The minimization procedure is implemented through a Nelder-Mead routine.
[45] The weighing procedure can also be implemented by choosing forward-time τ_f and backward-time τ_b intervals of integration such that strong minima are observed on $L_{f,b}$.
[46] The amplitude of the TS trajectory decreases with increasing barrier driving frequency. This characteristic behavior occurs as the TS trajectory is constructed using information from the barrier motion in the infinite future, and infinite past, in order to remain bounded to the energetic barrier top. As the barrier motion approaches stagnation, the amplitude of the TS trajectory approaches that of the barrier top.
[47] A. Sethi and S. Keshavamurthy, Phys. Rev. A **79**, 033416 (2009).